communications chemistry

Review article

https://doi.org/10.1038/s42004-024-01278-0

Post-spinel-type AB_2O_4 high-pressure phases in geochemistry and materials science

Masaki Akaogi [1,2] ✉, Takayuki Ishii[3] & Kazunari Yamaura [4]

Post-spinel-type AB_2O_4 compounds are stable at higher pressures than spinel phases. These compounds have garnered much interest in geo- and materials science for their geochemical importance as well as potential application as high ionic conductors and materials with strongly correlated electrons. Here, large-volume high-pressure syntheses, structural features and properties of post-spinels are reviewed. Prospects are discussed for future searches for post-spinel-type phases by applying advanced large-volume high-pressure technology.

Spinel-structured AB_2O_4 compounds are of great interest in geoscience and materials science. The name "spinel" is derived from the mineral name, $MgAl_2O_4$ spinel. The spinel-type structure of AB_2O_4 consists of almost cubic-closed packing array of O^{2-} with interstitial 4- and 6-fold coordination sites in which *A* and *B* cations are accommodated. Most of spinel-type AB_2O_4 compounds have cubic symmetry, and their physical properties are equivalent along the three axes.

When a spinel-type AB_2O_4 compound is compressed under pressure at high temperature or at room temperature in some compounds, it transforms to a high-pressure phase or dissociates into an assemblage of decomposed phases, and these changes are associated with density increases from the spinel-type phase. An AB_2O_4 compound stable at higher pressure than the spinel-type is called a "post-spinel" phase. $CaFe_2O_4$-, $CaTi_2O_4$- and $CaMn_2O_4$-type structures with orthorhombic symmetry are well known as major post-spinel structures[1]. Hereafter, we abbreviate the $CaFe_2O_4$-, $CaTi_2O_4$- and $CaMn_2O_4$-types as CF-, CT- and CM-types, respectively. In contrast to the spinel-type structure, all the CF, CT- and CM-type structures in AB_2O_4 are composed of one-dimensional framework of BO_6 octahedra with *A* cations in 6- to 8-fold coordination sites[2–6]. These post-spinel-type phases are generally ~10% denser than the corresponding spinel phases. The structural details are discussed later.

We note that in solid Earth science the transformation of Mg_2SiO_4 ringwoodite, a typical spinel-type A_2BO_4 compound, which occurs at ~660 km depth in the Earth's mantle, is also named as the post-spinel transition[7]. The AB_2O_4 post-spinel phase is used as a term in both of geoscience and materials science.

In geoscience, it is widely accepted that oceanic lithospheres covered with oceanic crust which consist of the top of the solid Earth are subducted into the deep mantle. Sedimentary rocks on the oceanic lithospheres are also subducted together. Hereafter, the oceanic crust and sedimentary rocks are called as "crustal materials". Chemical compositions of the oceanic crust[8] and sedimentary rocks[9] are rich in SiO_2, Al_2O_3, Na_2O and K_2O, compared with the average mantle composition[10]. By the subduction of the oceanic lithospheres, pressure-induced phase transitions of constituent minerals of the crustal materials take place at high-pressure and high-temperature conditions in the Earth's interior.

To examine the phase transitions in the subducted crustal materials, phase relations of various silicate-aluminate systems and natural crustal materials have been investigated by high-pressure and high-temperature experiments. These studies have clarified that the CF-type phase is one of major high-pressure minerals in the subducted crustal materials[11–19]. A "NAL" (New ALuminous) phase which has approximately $2/3AB_2O_4{\cdot}1/3CB_2O_4$ composition and hexagonal symmetry is another major high-pressure phase in the crustal materials[16,20]. In the following, we include the NAL-type phase into the group of post-spinel phases. This is because, similarly to the CF-, CT- and CM-type structures, the NAL-type structure consists of one-dimensional arrays of BO_6 octahedra with 6- and 9-fold sites for *A* and *C* cations[21]. The structural characteristics of the CF-, CT-, CM- and NAL-type phases are accompanied with their interesting properties, as described below.

In this review, we first discuss recent developments in high-pressure and high-temperature experimental techniques, using large-volume high-pressure apparatus. Then, a variety of post-spinel-type oxide materials are tabulated, and crystal structural characteristics of the post-spinel-type compounds are discussed in terms of ionic radii of constituent cations. We describe some results on phase relations and properties on post-spinel phases of geochemical and mineralogical interest. Following this, the discussion shifts to the perspective of materials science, highlighting the importance of post-spinel-type compounds as highly ionic conducting materials and for their strongly correlated electronic properties.

[1]Department of Chemistry, Gakushuin University, Toshima-ku, Tokyo, Japan. [2]Geochemical Research Center, Graduate School of Science, The University of Tokyo, Bunkyo-ku, Tokyo, Japan. [3]Institute for Planetary Materials, Okayama University, Misasa, Tottori, Japan. [4]Research Center for Materials Nanoarchitectonics (MANA), National Institute for Materials Science, Tsukuba, Ibaraki, Japan. ✉e-mail: masaki.akaogi@gakushuin.ac.jp

Recent developments in high-pressure and high-temperature experimental techniques using large-volume apparatus

In solid Earth science, high-pressure and high-temperature experiments are indispensable to simulate P, T conditions of the Earth's interior in laboratories, and in materials science they are valuable to synthesize novel materials which cannot be formed at atmospheric pressure. In these research fields, large-volume high-pressure apparatus such as a cubic anvil-type apparatus and a Kawai-type double-staged multi-anvil press are widely used. The name "large-volume apparatus" is derived from comparison with relatively small volume apparatus, particularly a diamond anvil cell (DAC). Although the laser-heated DAC enables to generate pressure more than 300 GPa and temperature higher than 5000 °C, the sample weight of the DAC experiment is less than order of 1 μg[22]. The large-volume high-pressure apparatus make it possible to synthesize a sample of more than 10^3–10^7 times larger volume than that available by the DAC in the same pressure range.

Figure 1 illustrates the cubic anvil press and Kawai-type multi-anvil apparatus together with their typical cell assemblies. In the cubic anvil press, a pressure-medium cube is compressed by six anvils. In the Kawai-type multi-anvil apparatus, six 1st-stage (outer) anvils compress eight 2nd-stage (inner) anvils. The eight inner anvils whose corner is truncated into a regular triangular face compress an octahedral pressure-medium. Generally, the cubic anvil press is used up to ~10 GPa, and the Kawai-type multi-anvil press up to ~25 GPa, to synthesize a large amount of polycrystalline sample in a single experimental run at high pressure and high temperature. In the cubic anvil press and Kawai-type multi-anvil apparatus, samples of several ten grams can be synthesized at pressures up to ~5–10 GPa, and those of up to several ten milligrams by using the Kawai-type apparatus at ~25 GPa at high temperature conditions. More details are given in the literature[23,24].

The large-volume presses have several other advantages: the precise control of pressure and temperature and the relatively uniform temperature distribution in the sample chamber using a furnace inside the pressure medium. Generally, in the experiments using the large-volume apparatus, a starting material is charged in a noble metal capsule such as Pt, Au and Re, which is placed in the central part of pressure medium. The capsule with the sample in the pressure medium is first compressed at room temperature to a desired pressure, and then temperature is elevated by supplying electric power to the heater. After being kept at the P, T condition for a certain period, e.g., several minutes to several hours depending of temperature, the sample is quenched under pressure by shutting off the heating power, and is recovered after release of pressure. This experimental procedure is called the sample-quenching method, allowing us to recover a high-pressure phase keeping its crystal structure under high pressure and high temperature.

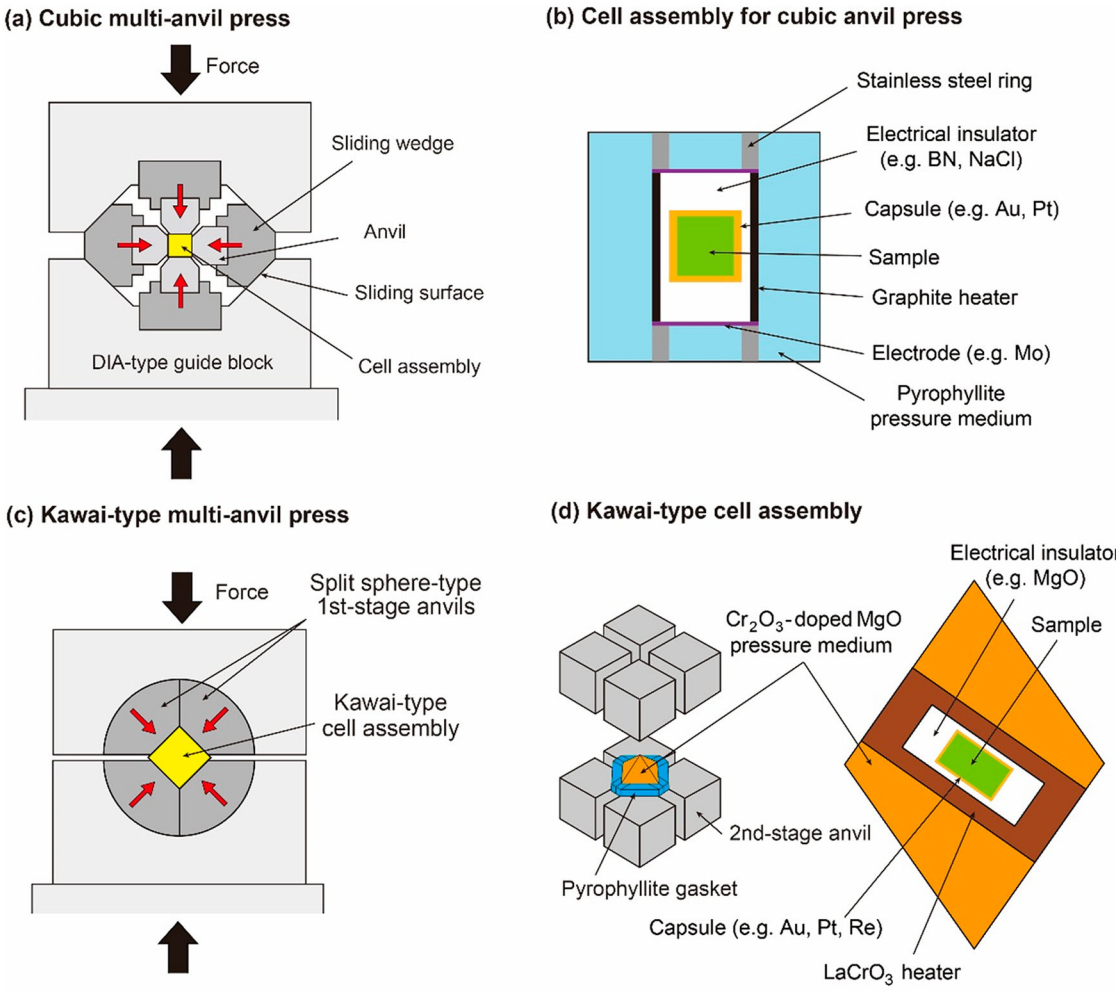

Fig. 1 | High-pressure experimental techniques using the large-volume apparatus. (**a**, **b**) the cubic multi-anvil press and the typical cell assembly. (**c**, **d**) the Kawai-type multi-anvil press and the cell assembly. The cubic multi-anvil press is generally used for experiments up to about 10 GPa. The DIA-type guide block in (**a**) is also called the Osugi-type[47]. The Kawai-type multi-anvil press is applied for experiments generally up to about 25 GPa. The cubic multi-anvil press can be scaled up and combined with the Kawai-type cell assembly to generate pressures up to 65 GPa. A thermocouple, not shown in (**b**) and (**d**), is inserted into each of the cell assemblies to monitor the sample temperature.

Single-phase materials with large quantities such as several tens of milligrams to several tens of grams synthesized at high pressure and high temperature are usually needed for accurate measurements of their physical and chemical properties. For example, thermodynamic properties (enthalpies, entropies and heat capacities) of high-pressure silicates which are stable in the Earth's interior have been measured at ambient pressure, using the quenched samples of several tens of milligrams to several grams[25–31]. Polycrystalline superhard materials have been synthesized using the multi-anvil techniques, such as nano-polycrystalline diamond with several gram quantity[32,33].

By using the large-volume apparatus, synthesis of single-crystals of several tens to hundreds μm in size is easily made in a pressure range up to ~25 GPa, and are recovered at ambient conditions[34,35]. These large single-crystals can be used for single-crystal X-ray diffraction structure analysis and spectroscopic measurements. Especially, combination of such a single-crystal with DAC techniques have contributed to significant progress on characterization of geomaterials at high pressure by measurements such as Brillouin scattering, Raman, and Mössbauer spectroscopies[36,37].

Control of fugacities of oxygen, water, etc., in the sample chamber can be made in the experiments using the large-volume apparatus. For example, oxygen fugacity is controlled by using oxygen buffers such as Fe-FeO and Re-ReO_2 or by adding oxidizing agents such as $KClO_3$, $KClO_4$ and $NaClO_3$ which release oxygen at high temperature. These methods allow us to synthesize single- or mixed-valence cation (Fe^{2+} and/or Fe^{3+})-bearing compounds and abnormal valence cation (e.g., Fe^{4+})-bearing compounds[38–40]. Also, single-crystals of a high-pressure phase with up to several mm in size can be made by mixing an appropriate flux such as water and NaCl with the starting material[41–43]. The combination of large-volume apparatus with synchrotron X-ray radiation is a powerful method for in situ observation of structural changes of the sample[44,45]. The details of the in situ X-ray observation method are found in the literature[23].

In the experiments of the Kawai-type double-staged multi-anvil apparatus, tungsten carbide (WC) anvils are usually adopted for the second-stage anvils. Before the 2000s, generated pressure was limited up to ~25 GPa at temperature of ~1000–2000 °C, using the Kawai-type multi-anvil apparatus. Recently, the pressure limit was extended to ~65 GPa at room temperature and ~50 GPa at temperature up to ~1700 °C by using newly invented hardened WC anvils with effective control of pressure and temperature generation efficiencies[46,47]. Samples with half milligrams and ~50–100 μm-sized single-crystals have been synthesized, allowing to perform crystal structure analysis and optical measurements under pressure in a DAC[48,49]. This expansion of pressure provides new opportunities for studies on phase transitions and physical properties of the materials in the deep part of the Earth's mantle and for synthesis of a wider range of novel materials.

Crystal structures of post-spinel phases

$CaFe_2O_4$-, $CaTi_2O_4$- and $CaMn_2O_4$-type phases

Table 1 summarizes post-spinel-structured AB_2O_4 high-pressure phases of Earth's minerals studied in geoscience, and also some post-spinel-type minerals stable at atmospheric pressure. Table 2 lists post-spinel-type AB_2O_4 phases synthesized at atmospheric and high pressure from the interest of materials science.

$CaFe_2O_4$ (CF)-, $CaTi_2O_4$ (CT)- and $CaMn_2O_4$ (CM)-type structures, all of which are orthorhombic in symmetry, are the post-spinel structures for various AB_2O_4 compounds. Figure 2a, b illustrates the CF-type (*Pnma*) and CT-type (*Cmcm*) structures, respectively, where symbols in parentheses represent space groups. Both of the structures consist of double chains of edge-sharing BO_6 octahedra, which contain 6-fold coordinated *B* cations by O^{2-}. The double chains are running parallel to one of the orthorhombic cell axes. Four double chains form a tunnel-like space by corner-sharing of BO_6 octahedra. In the tunnel spaces, *A* cations are accommodated in 8-fold coordinated bicapped prism sites (for the CT-type, see more details below). Although the two structures in Fig. 2a, b look very similar, arrangements of the double chains of octahedra are different between CF- and CT-type structures, as shown by the difference in space group. The $CaMn_2O_4$ (CM)-type structure (*Pbcm*) is essentially the same as CT-type in the arrangement of octahedra, but it is different from CT-type because octahedra of the CM-type structure are distorted by Jahn-Teller active ions such as Mn^{3+} ($3d^4$)[6]. Due to the distortion, the space group of CM-type is lower than that of CT-type.

When we look at the CF- and CT-type structures in more detail, the coordination environments of *A* cations in both the structures are different. Structure analysis of CF-type $MgAl_2O_4$[50] indicated that eight *A*-O distances in the 8-fold coordinated bicapped prism sites spread over a wide range, 2.13–2.49 Å. However, in the CT-structured $MgAl_2O_4$[49], eight *A*-O distances are divided into two groups; two long *A*-O distances of 2.56 Å and six short ones of 2.02–2.21 Å. The latter six *A*-O bonds form a trigonal prism site. Therefore, *A* cations in the CT-type is regarded as practically in the 6-fold trigonal prism sites rather than the 8-fold sites. These structural differences imply that the CF-type structure is more flexible to accommodate cations of a wider range in size, compared with those in the CT-type[51]. The differences are also reasons that CF-type phase forms at a wide P, T range in the Earth's deep interior of multi-component systems, as described in section "Post-spinel phases in geochemical and mineralogical interest", and that CT-type phase does not frequently appear even in compositionally simple systems.

NAL-type phase

In some binary AB_2O_4-CB_2O_4 systems, a high-pressure phase with an intermediate composition, $2/3AB_2O_4{\cdot}1/3CB_2O_4$ or $A_2CB_6O_{12}$, is stable and has a structure with hexagonal symmetry. This $A_2CB_6O_{12}$ phase is the NAL phase ($P6_3/m$), and its structure is shown in Fig. 2c[21]. The structural framework of the $A_2CB_6O_{12}$ phase is double chains of edge-sharing BO_6 octahedra running parallel to the c-axis, like CF-, CT- and CM-types. The NAL phase structure, however, has three different sites for cations. They are small octahedral sites for *B*, middle-sized 6-fold trigonal sites for *A*, and large 9-fold sites for *C*. As shown in Fig. 2c, the 9-fold and 6-fold trigonal sites are formed in tunnel spaces surrounded by the double chains of octahedra. The occupancy of the 9-fold sites is 0.50 in the $A_2CB_6O_{12}$ composition.

Post-spinel phases in geochemical and mineralogical interest

Experimental studies on phase transitions of various spinel-type AB_2O_4 compounds at high pressure and high temperature have indicated several different pathways from spinel-type to post-spinel-type. The first one is that a spinel-type AB_2O_4 directly transforms to a post-spinel-type phase. For example, spinel-type $MnCr_2O_4$ transforms to CF-type phase at ~10 GPa at 1000–1200 °C[51]. Other types are that a spinel-type AB_2O_4 first dissociates into two phases, which then combine into a single AB_2O_4 post-spinel phase at higher pressure. Three kinds of the dissociated phase assemblages have been reported so far; rock-salt (Rs)-type *AO* + corundum (Cor)-type B_2O_3 (e.g., $MgAl_2O_4$, FeV_2O_4), modified-ludwigite (mLd)-type $A_2B_2O_5$ + Cor-type B_2O_3 (e.g., $MgAl_2O_4$, $FeCr_2O_4$), and $CaFe_3O_5$-type $A_2B_2O_5$ + Cor-type B_2O_3 (e.g., $Fe^{2+}Fe^{3+}{}_2O_4$)[52–55].

In geoscience, precise phase relations of geomaterials at high pressure and high temperature are essential to apply the results to the Earth's interior. The large-volume high-pressure techniques are necessary to obtain the accurate phase relations, because of precise control of pressure and temperature, compared particularly with the DAC experiments. In the following, we show, as examples, high-pressure and high-temperature phase relations in $MgAl_2O_4$ and those in the $CaAl_2O_4$-$MgAl_2O_4$ system (Fig. 3) determined by the large-volume presses.

Figure 3a exhibits the phase relations in $MgAl_2O_4$ up to ~35 GPa and ~2700 °C, based on the experimental data by the large-volume apparatus[49,53,56–58]. Below ~2000 °C, spinel-type $MgAl_2O_4$ dissociates into Rs-type MgO + Al_2O_3 Cor at ~15–18 GPa, and they combine into CF-type at ~27 GPa. Above ~2000 °C, however, spinel decomposes into mLd-type + Cor at ~20–22 GPa, which combine into CF-type $MgAl_2O_4$ phase at ~26 GPa. The CF-type phase further transforms to CT-type at around

Table 1 | Post-spinel-type high-pressure phases of Earth's minerals

Phase	Structure	Transition P,T		Structure	Ref.
		P(GPa)	T (°C)	analysis	
$MgAl_2O_4$	CF	27	1600	R	50,57
$MgAl_2O_4$	CT	27	2500	SC	49
$MgCr_2O_4$	CT	18	1400	R	99
$FeCr_2O_4$	CF[a]	18	1300	P	54
$FeCr_2O_4$	CT	28	1300	R	54
$NaAlSiO_4$	CF	19	1200	R	62,91
$CaAl_2O_4$	CF	8	1200	R	57,100
$CaFe_2O_4$	CF	0	1250	SC	2
$CaTi_2O_4$	CT	0	1000	SC	5
$CaMn_2O_4$	CM	0	1250	SC	3
$CaMn_2O_4$	CT[a]	30	25	R	6
Mn_3O_4-II	CM	11	1000	R	101,102
$Mg_2CaAl_6O_{12}$	NAL	16	1200	R	21,64
$Mg_2NaAl_5SiO_{12}$	NAL	14	1500	R	65,66
$Mg_2KAl_5SiO_{12}$	NAL	16	1500	R	64,66

These phases are stable in the Earth's interior as endmembers of mineral solid solutions. CF: $CaFe_2O_4$-type, CT: $CaTi_2O_4$-type, CM: $CaMn_2O_4$-type, NAL: NAL-type, R: Rietveld structure refinement, SC: single-crystal structure analysis, P: powder X-ray diffraction method.
[a]Unquenchable phase at atmospheric pressure.

30–35 GPa[49,59–61]. Although the transition boundary between CF- and CT-phases has not yet been fully constrained, the CT-type has been synthesized at 27 GPa and 2500 °C[49] and at 50 GPa and 1700 °C[61]. We note that the first structure analysis of CT-type $MgAl_2O_4$ was made using a single-crystal of ~40 μm in size synthesized at 45 GPa and ~1700 °C by the advanced multi-anvil techniques[49]. Recovered $MgAl_2O_4$ samples from the region of ~26–30 GPa above ~2200–2500 °C have a novel structure different from CF- and CT-types[49,53], which will be discussed later.

Some AB_2O_4 phases which do not have the spinel structure at atmospheric pressure transform to post-spinel-type phases at high pressure. $CaAl_2O_4$ and $NaAlSiO_4$ have the stuffed-tridymite structure at atmospheric pressure, and both the phases transform to CF-type at ~10 and ~20 GPa, respectively, at 1200 °C via some intermediate phases[57,62].

Phase transitions among CF-, CM- and CT-type phases have also been observed. In $FeCr_2O_4$, a spinel-type phase decomposes at ~18 GPa and 1300 °C into mLd + Cor, and they combine into CF-type, which further transforms to CT-type at ~28 GPa[54]. We note that the high-pressure $FeCr_2O_4$ polymorphs and mLd-type $Fe_2Cr_2O_5$ were successfully synthesized under controlled oxygen fugacity with the Fe-FeO buffer in the multi-anvil experiments described in section "Recent developments in high-pressure and high-temperature experimental techniques using large-volume apparatus". The CF-type $FeCr_2O_4$ is not quenchable but changes during decompression into a new, modified CF-type phase with a five-fold coordination for A-site cations in the tunnel space. By room temperature compression, CM-type $CaMn_2O_4$ transforms discontinuously at ~30 GPa to CT-type, which is not quenchable and back-transforms to the CM-type on release of pressure[6], indicating that the Jahn-Teller distortion of MnO_6 octahedra is suppressed at high-pressure conditions in the CT-type phase.

New-structured post-spinel phases were recently discovered in $MgAl_2O_4$ and $MgFe_2O_4$ as recovered samples from 20–27 GPa and 1200–2500 °C[49,63]. They have *B*-site polyhedral frameworks and tunnel structures which are different from those of the CF-, CT, and CM-types, It is expected that further new-structured post-spinel phases can be discovered by applying the advanced high-pressure technology.

Figure 3b shows a schematic diagram of phase relations in the $CaAl_2O_4$-$MgAl_2O_4$ system up to 32 GPa at 1200 °C[57,64]. $CaAl_2O_4$ and $MgAl_2O_4$ transform to CF-type at ~8 and ~28 GPa, respectively[57]. In an

Table 2 | Post-spinel-type phases synthesized at atmospheric pressure and at high pressure in the interest of materials science

Phase	Structure	Synthesis P,T		Structure	Ref.
		P(GPa)	T (°C)	analysis	
CaV_2O_4	CF	0	1200	R	103
$Ca_{2/3}Mn_2O_4$	CF	0	1200	R	104
$SrTl_2O_4$	CF	0	900	R	105
$SrLn_2O_4$ (Ln = Gd, Ho,Yb)	CF	0	1500	R	106
$BaLn_2O_4$ (Ln = La, Nd, Sm, Gd, Ho, Yb)	CF	0	820–1000	SC	107
$LiVTiO_4$	CF	0	390	R	89
$LiCrTiO_4$	CF	0	450	R	89
$LiFeTiO_4$	CF	0	350	R	108
$LiRhTiO_4$	CF	0	450	R	89
$LiMn(Sn_{1-x},Ti_x)O_4$ (x = 0, 0.3, 0.45)	CF	0	350	R	89
$LiM_{0.5}Ti_{1.5}O_4$ (M = Mg, Co, Fe)	CF	0	350–390	R	89
$NaTi_2O_4$	CF	0	1200	SC	84
$NaRu_2O_4$	CF	0	950	SC	94
$NaCrTiO_4$	CF	0	900	R	88
$NaRhTiO_4$	CF	0	950	R	88
$NaV_{1.25}Ti_{0.75}O_4$	CF	0	700	R	109
$NaCrSnO_4$	CF	0	1000	R	88
$NaMnSnO_4$	CF	0	1200	R	88
$NaInSnO_4$	CF	0	1200	R	88
$NaVSnO_4$	CF	0	750	R	109
$Na_{0.56}Ti_{0.28}Fe_{1.72}O_4$	CF	0	1220	SC	110
$(A,Bi)_{2/3-x}Rh_2O_4$ (A = REE)	CF	0	1000	SC	111
$NaAlGeO_4$	CF	12	900	P	112
$MgMn_2O_4$[a]	CM	15	25	R	86
MFe_2O_4[a] (M = Mg, Fe, Zn)	CT	25-40	25	R	113
$MnCr_2O_4$	CF	10	1200	R	51
FeV_2O_4	CT	11	1200	R	51
$ZnGa_2O_4$[a]	CM	55	25	P	79
$CuRh_2O_4$	CF	4	900	P	114
$CdRh_2O_4$	CF	6	1400	R	115
$CdCr_2O_4$	CF	10	1100	R	116
$CaCo_2O_4$	CF	6	1500	R	117
$CaRh_2O_4$	CF	6	1500	SC	96
NaV_2O_4	CF	6	1700	SC	43
$NaMn_2O_4$	CF	4.5	1100	SC	92
$NaRh_2O_4$	CF	6	1500	R	96
$LiMn_2O_4$	CF	6	1200	R	82
$NaLi_2Ru_6O_{12}$	NAL	0	1100	SC	90
$KLi_2Ru_6O_{12}$	NAL	0	1100	SC	90
$SrBe_2Rh_6O_{12}$	NAL	0	1000	P	93
$SrMg_2Rh_6O_{12}$	NAL	0	1000	P	93

REE rare earth element.
These phases synthesized in laboratories are not present in the Earth's interior. CF: $CaFe_2O_4$-type, CT: $CaTi_2O_4$-type, CM: $CaMn_2O_4$-type, NAL: NAL-type, R: Rietveld structure refinement, SC: single-crystal structure analysis, P: powder X-ray diffraction method.
[a]Unquenchable phase at atmospheric pressure.

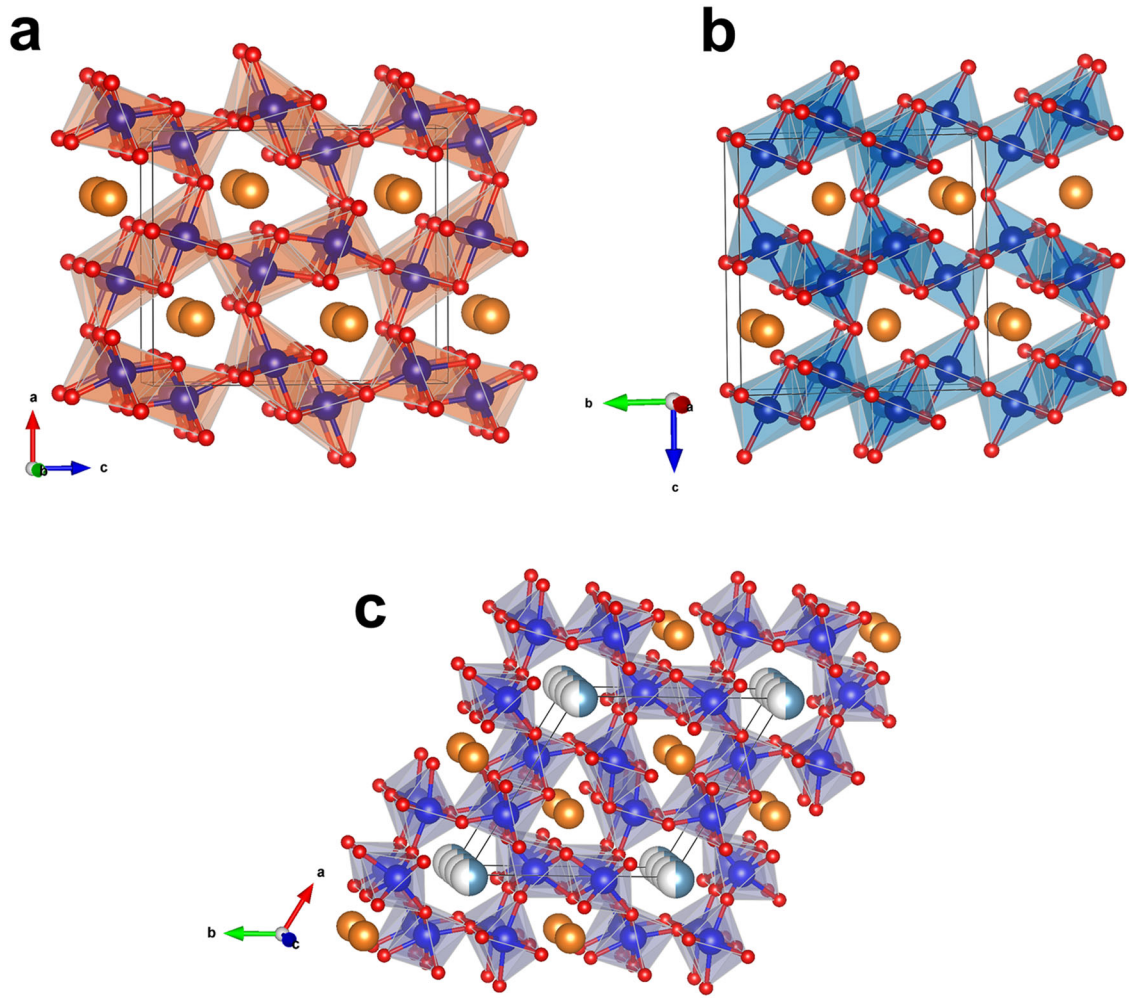

Fig. 2 | Crystal structures of post-spinel phases. (**a**) $CaFe_2O_4$(CF)-type, (**b**) $CaTi_2O_4$(CT)-type, and (**c**) NAL-type structures. In (**a**) and (**b**) of the post-spinel AB_2O_4 phases, the large brown spheres and small red spheres express *A* and O, respectively. Middle-sized blue spheres in the octahedra are *B*. In (**c**) of the NAL-type $A_2CB_6O_{12}$ phase, large blue/silver spheres and small red spheres represent *C* (half occupancy) and O, respectively. Brown spheres are *A*, while blue spheres in the octahedra are *B*. Structure data: (**a**) CF-type $MnCr_2O_4$[51], (**b**) CT-type $MgCr_2O_4$[99], and (**c**) $Mg_2CaAl_6O_{12}$[21]. Drawn with VESTA[118].

approximate composition of $1/3CaAl_2O_4{\cdot}2/3MgAl_2O_4$ or $CaMg_2Al_6O_{12}$, a NAL-type phase with the compositional width of ~5 mol % is stable in the system above ~16 GPa. In the $NaAlSiO_4$-$MgAl_2O_4$ and $KAlSiO_4$-$MgAl_2O_4$ systems, NAL-type phases are stable above ~15 GPa at 1200–1600 °C in a wide compositional range up to ~20 mol %[64,65]. Composition analysis[65] and structure analysis[66] of the NAL phase solid solutions in the $NaAlSiO_4$-$MgAl_2O_4$ system revealed that the occupancy in the 9-fold sites deviated from 0.50 to ~0.45. Tables 1 and 2 include the various NAL-type phases.

As described in Introduction, post-spinel-type phases of aluminous silicate compositions are stable in the Earth's lower mantle conditions. In addition to the simplified silicate-aluminate systems discussed above, a number of high-pressure and high-temperature experimental studies on natural crustal compositions indicated that CF- and NAL-type phases become stable as major aluminous phases in the lower mantle conditions[11–13,15–18,67,68]. In particular, the CF-type phase is stable in the pressure range of ~24–135 GPa in the whole lower mantle (~660–2900 km in depth). In the crustal materials in the lower mantle, $NaAlSiO_4$ and $MgAl_2O_4$ are two major components in the CF-phase[13,16–19]. The NAL-type phase contains not only the two components but also $KAlSiO_4$ component[64,66,67]. In contrast, the other major minerals stable in the lower mantle conditions, i.e., Mg-rich bridgmanite with the orthorhombic-perovskite structure, rock-salt type (Mg, Fe)O ferropericlase, $CaSiO_3$-rich cubic-perovskite phase, and SiO_2 stishovite, contain almost no Na^+ and K^+ in the structures[17,19,69].

Among geochemically abundant elements of the solid Earth, Na^+ and K^+ play important roles in melting and differentiation in the Earth's interior. Therefore, subduction of crustal materials containing CF- and NAL-type phases into the lower mantle is one of most important processes for circulation of materials including the alkali elements in the Earth's interior[70]. In addition, host-phases of K^+ in the deep mantle are of significant importance in the Earth's thermal history, because a long-lived radiogenic element ^{40}K is a major heat source in the Earth's interior[71]. A K-rich NAL phase with the approximate composition of $KMg_2Al_5SiO_{12}$ is stable even at ~135 GPa and ~2000 °C, which correspond almost to the Earth's core-mantle boundary conditions[72]. This result suggests that the NAL phase may be a candidate of high-pressure minerals which transport K from the mantle into the core[73].

Physical properties of CF-, CT- (if exists) and NAL-type phases in geochemical systems, such as electrical conductivity and rheology, may provide new insights for understanding of the structure and dynamics of the Earth's interior. As will be discussed in section "Post-spinel phases in materials science", the post-spinel phases in geochemical systems also are expected to have potentially distinctive transport properties, because of possible high ionic conduction (fast cation diffusion) through and large thermal vibration of cations in the tunnel structures. Although transport properties of dominant minerals in the mantle such as olivine and bridgmanite have been investigated[74], no such studies have been reported on the

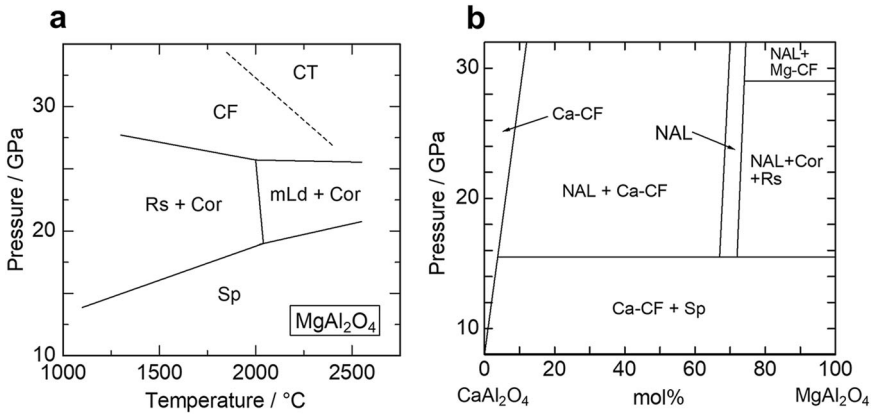

Fig. 3 | High-pressure and high-temperature phase relations of some typical post-spinel phases. (**a**) $MgAl_2O_4$, and (**b**) the $CaAl_2O_4$-$MgAl_2O_4$ system at 1200 °C. In (**a**), Sp: $MgAl_2O_4$ spinel, Rs: rock-salt-type MgO, Cor: Al_2O_3 corundum, mLd: modified ludwigite-type $Mg_2Al_2O_5$, CF: $CaFe_2O_4$-type $MgAl_2O_4$, CT: $CaTi_2O_4$-type $MgAl_2O_4$. In (**b**), Ca-CF: Ca-rich $CaFe_2O_4$-type solid solution, Mg-CF: $CaFe_2O_4$-type $MgAl_2O_4$, NAL: NAL-type solid solution.

post-spinel phases in the geochemical systems. Therefore, these studied will be paid more attention in solid Earth science in near future.

Crystal chemical characteristics of post-spinel phases in terms of cation radii

Figure 4a exhibits structure types of a variety of post-spinel $A^{2+}B^{3+}{}_2O_4$ compounds synthesized at atmospheric and high pressure, in terms of 8-fold coordinated A^{2+} radius, R(A^{2+}), and 6-fold coordinated B^{3+} radius, R(B^{3+}). We use Shannon's ionic radii[75] throughout this article. The data in Fig. 4a, b are based on those summarized in Tables 1 and 2, in addition to those from other literature shown in the figure caption. All the post-spinel phases in Fig. 4 are quenchable to ambient conditions.

As shown in Fig. 4a, CF-type $A^{2+}B^{3+}{}_2O_4$ compounds with R(A^{2+}) and R(B^{3+}) smaller than ~1.1 and ~0.65 Å, respectively, can be synthesized only at high pressure. This is consistent with the ideas that radii of these A^{2+} and B^{3+} ions are too small at atmospheric pressure to occupy the cation sites coordinated by O^{2-} anions in the post-spinel-type $A^{2+}B^{3+}{}_2O_4$ structures, and that relatively large O^{2-} is more compressible than relatively small A^{2+} and B^{3+}. In Fig. 4a, CM-type phases appear only in $A^{2+}Mn^{3+}{}_2O_4$ compounds, because of the Jahn-Teller active Mn^{3+} ions. The CM-type phases may be included in the CT-type group, as discussed in section "$CaFe_2O_4$-, $CaTi_2O_4$- and $CaMn_2O_4$-type phases". Figure 4a shows that CF-type $A^{2+}B^{3+}{}_2O_4$ phases are formed in wide ranges of A^{2+} and B^{3+} radii, ~0.89–1.42 Å and ~0.53–1.03 Å, respectively. On the other hand, CT-and CM-type high-pressure phases are synthesized only in the region of R(A^{2+}) smaller than ~0.95 Å. These characteristics can be explained by the structural difference between CF- and CT-types, i.e., A^{2+} cations in CF-type are accommodated in the larger 8-fold coordinated bicapped-triangular prism sites, while those in CT-type are in the smaller 6-fold triangular prism sites, as described in section "$CaFe_2O_4$-, $CaTi_2O_4$- and $CaMn_2O_4$-type phases".

Figure 4b shows the structure types of $A^+(B^{3+}B^{4+})_2O_4$ compounds in terms of R(A^+) and the average of R(B^{3+}) and R(B^{4+}), where A^+ is an 8-fold coordinated cation and B^{3+} and B^{4+} are 6-fold ones. The figure exhibits that CF-type $A^+(B^{3+}B^{4+})_2O_4$ compounds with R(A^+) and 1/2(R(B^{3+}) + R(B^{4+})) smaller than ~1.18 and ~0.62 Å, respectively, can be synthesized only at high pressure, though the data are limited. This tendency is similar to that in Fig. 4a. In addition, the structures of $LiMn_2O_4$, $NaMn_2O_4$ and $NaMnSnO_4$ are not CM-type but CF-type. This indicates that the CF-type structure is formed, even when half of B cations are Jahn-Teller active ions, further supporting the more flexible structure of CF-type than CT/CM-type.

For a given $A^{2+}B^{3+}{}_2O_4$ or $A^+(B^{3+}B^{4+})_2O_4$ composition, the diagrams in Fig. 4 can be used to predict whether the post-spinel-type phase can be synthesized at atmospheric pressure or is stable only at high pressure and which phase is stable between CF-type and CT-type (including CM-type). These may help us design new post-spinel phases with expected structure and properties. For example, it may be suggested from Fig. 4a that spinel-type $ZnCr_2O_4$ transforms to CT-type rather than CF-type at high pressure.

Although stability of some post-spinel phases of AB_2O_4 have been studied by theoretical methods such as the density functional theory (DFT)[76,77], such investigations are still limited. The DFT studies revealed that $MgAl_2O_4$ spinel first dissociated at ~15 GPa into MgO + Al_2O_3 corundum, which then combined into CT-type at ~45 GPa, though CF-type $MgAl_2O_4$ and modified ludwigite-type $Mg_2Al_2O_5$ were not taken into account in the calculations (see Fig. 3a). A first-principles calculation study suggested that spinel-type $ZnGa_2O_4$ transformed to CM-type at 39 GPa and spinel-type $ZnAl_2O_4$ to CF-type at 33 GPa[78]. The in situ X-ray diffraction experiments showed that CM-type of $ZnGa_2O_4$ occurs at ~55 GPa[79], though the post-spinel transition in $ZnAl_2O_4$ has not yet been found experimentally. Further theoretical studies on post-spinel transitions in a variety of AB_2O_4 compounds are desirable to compare with previous experimental results and predict future directions of experimental studies.

Post-spinel phases in materials science

Ionic conduction

Post-spinel AB_2O_4 phases are of significant interest not only in geoscience but also in materials science. The one-dimensional arrangement of A cations in the tunnel spaces of the post-spinel structures suggests the potential for ionic conduction through the tunnels[80,81]. However, the extent of ionic mobility in these structures remains debated, necessitating further experimental investigations.

Despite this uncertainty, some post-spinel-type AB_2O_4 compounds with redox-active B cations have garnered attention as potential high-performance cathode materials for rechargeable batteries due to their possible high cationic mobility. For instance, the spinel-to-CF transition in $LiMn_2O_4$ was first reported through high-pressure and high-temperature synthesis experiments[82]. The study showed that the polycrystalline sample synthesized at 6 GPa and 900–1500 °C has a CF-type structure with the composition of $Li_{0.92}Mn_2O_4$ and an activation energy barrier for ionic conduction approximately two-thirds that of spinel-type $LiMn_2O_4$, suggesting enhanced Li^+ mobility after the spinel-to-CF transition. Further synthesis studies revealed that stoichiometric CF-type $LiMn_2O_4$ could not be synthesized at 6 GPa and 600–1000 °C, with coexisting decomposition products such as Li_2MnO_3 affecting the rechargeable capacity[83]. These findings underscore the complexity and need for continued research to fully understand the ionic mobility and practical applications of post-spinel materials.

Recent studies have also synthesized CF-structured $NaMn_2O_4$ at 4.5 GPa and 1100 °C[84], demonstrating stable battery performance during Na^+ ion insertion and extraction[85]. Similarly, $MgMn_2O_4$ has shown a transition to a CM-type phase at 15 GPa at room temperature due to the Jahn–Teller distortion of $Mn^{3+}O_6$ octahedra[86]. Further studies on the CM-type $MgMn_2O_4$ concerning its ionic mobility are anticipated.

First-principles calculations indicate that CF-type AMn_2O_4 (A = Li, Na, Mg) compounds have lower energy barriers for the diffusion of Li^+, Na^+, and Mg^{2+} in tunnel spaces, compared to their CT- and CM-type

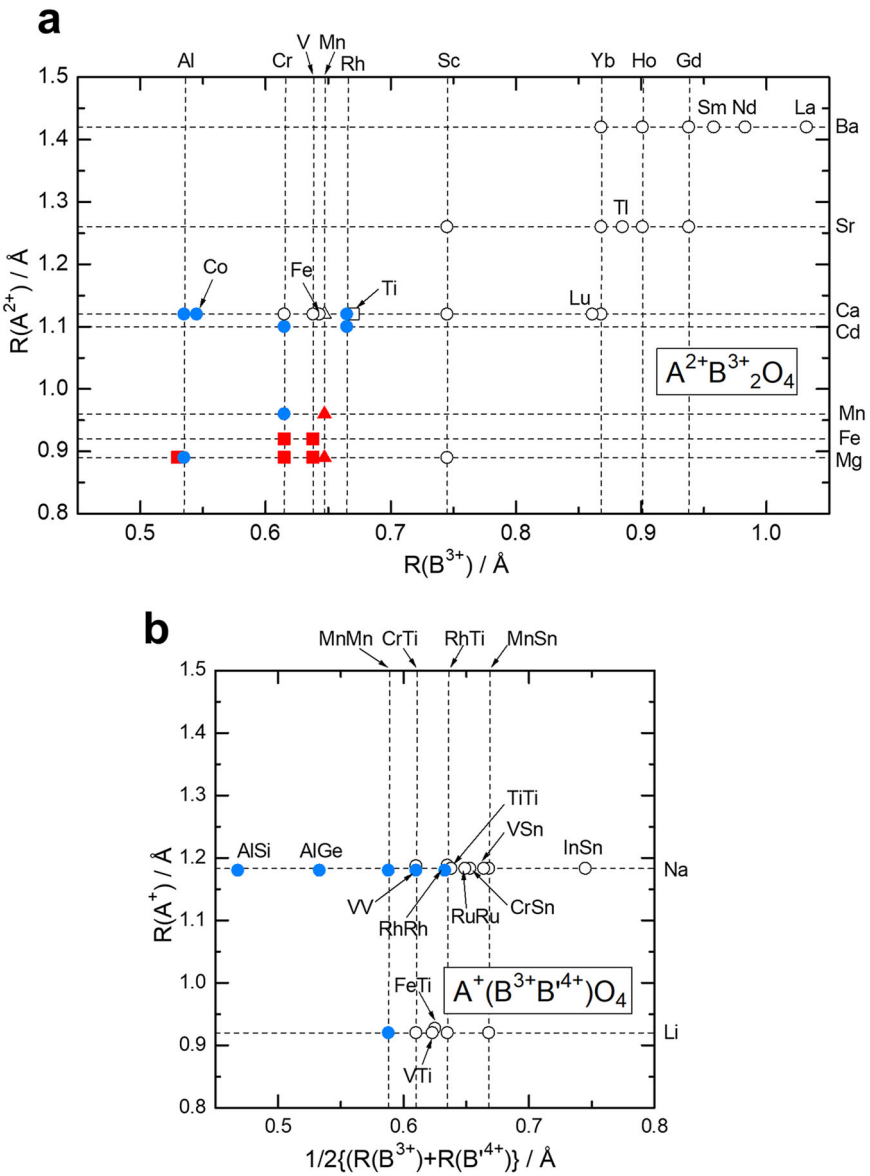

Fig. 4 | Crystal structure types of post-spinel phases in terms of cation radii. (**a**) $A^{2+}B^{3+}{}_2O_4$ and (**b**) $A^+(B^{3+}B'^{4+})_2O_4$ synthesized at atmospheric pressure (open symbols) and at high pressure (closed, blue and red symbols). Circles, squares and triangles: $CaFe_2O_4$(CF)−, $CaTi_2O_4$(CT)− and $CaMn_2O_4$(CM)-type phases, respectively. R(M^{n+}) in the vertical axes express cation radii of M^{n+} in 8-fold coordination, and those in the horizontal axes represent those in the 6-fold coordination[75]. Data are from Tables 1 and 2 and from the literature for $MgSc_2O_4$[119], $CaCr_2O_4$[120], $CaSc_2O_4$[121], $CaLu_2O_4$[122], $CaYb_2O_4$[122] and $SrSc_2O_4$[123].

counterparts[87], aligning with the structural flexibility of CF-type phases, as discussed in Section 3.

At atmospheric pressure and high temperature, several Na-bearing post-spinel compounds with the CF-type structure were recently synthesized, e.g., $NaB^{3+}TiO_4$ (B = Cr, Rh), $NaB^{3+}SnO_4$ (B = Mn, Cr, In), and related solid solutions[88]. The results significantly expanded the compositional space of Na-bearing CF-type phases synthesized at atmospheric pressure, providing helpful insights for searching potential battery electrode materials. Furthermore, several Li-containing post-spinel compounds with the CF-type structure were synthesized very recently at atmospheric pressure and high temperature from Na-bearing post-spinel counterparts by Li^+-Na^+ exchange process, e.g., $LiB^{3+}TiO_4$ (B = V, Cr, Rh) and $LiMnSnO_4$[89]. The results suggest that the Li-post-spinel compounds may be promising candidates for new Li-ion energy storage materials. High-pressure synthesis methods may expand the compositional space further and deepen our understanding.

NAL-type phases are also of interest in materials science. As shown in Fig. 2c, the NAL-type structure has three different sites for cations: small 6-fold octahedral sites, middle 6-fold trigonal sites, and large 9-fold sites. The NAL-type phases have been synthesized not only in aluminous silicates described in section "NAL-type phase" but also in other compositions such as platinum-group metal oxides. Several ruthenium oxides, $ALi_2Ru_6O_{12}$ (A = Na, K, Ca, Sr), were synthesized at atmospheric pressure at 1100 °C, and the structure analysis indicated that $KLi_2Ru_6O_{12}$ and $NaLi_2Ru_6O_{12}$ have the NAL-type structure[90]. In these phases, Ru and Li are placed in the octahedral and middle-sized 6-fold trigonal sites, respectively, while K and Na occupy the large 9-fold sites. Na^+ is incorporated in the large 9-fold coordination site of the NAL-type structure in both aluminous silicates and ruthenium oxides. Structure analysis of NAL-type $Na_{1.04}Mg_{1.88}Al_{4.64}Si_{1.32}O_{12}$ indicated that the average Na-O distance in the 9-fold site is 2.64 Å[66], while those in the 8-fold sites in the CF-type $NaAlSiO_4$ and $NaMn_2O_4$ are 2.40 and 2.44 Å, respectively[91,92]. The large 9-fold sites in the tunnel spaces of the NAL structure may suggest potentially high Na^+ mobility in the structure.

Rhodium oxides $AA'Rh_6O_{12}$ (A = Sr, La, Bi, Pb; A' = Mg, Li, Be) with the NAL-type structure were also synthesized at atmospheric pressure at 1000–1100 °C. Their electrical and magnetic properties showed high electrical conductivity and a high Seebeck coefficient, suggesting they could be promising candidates for thermoelectric materials at high temperatures[93], as will be mentioned in the next section. High-pressure studies on the exploration of new NAL-type phases have not been active in materials science, but it is hoped that exploratory studies will progress. For example, expansion of the compositional range by using high-pressure methods may improve thermoelectric performance.

Strongly correlated properties

Recent advances in multi-anvil high-pressure experimental techniques have significantly advanced materials science. As discussed in section "Recent developments in high-pressure and high-temperature experimental techniques using large-volume apparatus", the large capacity of high-pressure synthesis technology has facilitated precise structural analysis and evaluation of strongly correlated physical properties through measurements such as electronic transport, magnetic properties, and thermal properties measurements, especially neutron scattering experiments that usually require sample masses in the order of several grams. The contribution of these advanced measurement technologies and the capacity to produce large high-pressure synthetic samples is noteworthy.

Research on large sample masses of post-spinel-type oxides synthesized under high-pressure conditions has highlighted their potential as materials with strongly correlated electronic properties. A particular focus has been on oxides exhibiting metallic conductivity, such as $NaRu_2O_4$[94]. Synthesized in 2006, $NaRu_2O_4$ is recognized as an unusual post-spinel-type oxide with metallic conductivity[95]. Recent studies have unveiled a significant correlation between dimerization and charge ordering, facilitated by the formation of metal-metal bonds[94]. Similarly, $NaRh_2O_4$, synthesized in 2005 as the first metallically conducting post-spinel oxide, has attracted considerable attention[96]. Theoretical calculations suggested that substituting Ca for Na in the post-spinel-type $NaRh_2O_4$ could significantly enhance its thermoelectric properties, targeting a ZT of approximately 0.79 at 250 K[97]. Here, the figure of merit ZT, which quantifies the efficiency of a material's thermoelectric power conversion, is defined as $ZT = S^2\sigma T/\kappa$, where S is the Seebeck coefficient, σ is the electrical conductivity, T is the absolute temperature, and κ is the thermal conductivity. However, initial experiments did not confirm these anticipated improvements[96], highlighting the need for further investigation into their potential as thermoelectric materials.

Post-spinel-type NaV_2O_4, first synthesized in 2007 with the flux growth method by large-volume high-pressure experiments, exhibits a half-metallic ground state[43], and was recently proposed as a magnetic topological material[98], making it promising for spintronic applications. The growth of high-quality single crystals under high pressure, utilizing large sample space, is crucial for further investigation of these properties.

Conclusions and outlook

High-pressure and high-temperature experimental techniques using the large-volume apparatus have been extensively developed in the last two decades. In a single experimental run by the large-volume press, a high-pressure phase of several ten grams can be synthesized at pressures up to ~10 GPa and several ten milligrams up to ~25 GPa under controlled atmosphere. Furthermore, a sample of approximately half milligram has been able to synthesize at pressures up to ~50 GPa, as described in section "Recent developments in high-pressure and high-temperature experimental techniques". Single-crystals large enough for structure analysis and spectroscopic studies can be synthesized in the whole pressure range shown above. These advancements in high-pressure and high-temperature technology have significantly impacted both geoscience and materials science. In recent decades, various new AB_2O_4 post-spinel phases have been synthesized at high-pressure and high-temperature conditions, and the structures have been analyzed and their physical and chemical properties have been measured. This review article summarized progress of the research on these post-spinel-type compounds in geoscience and materials science.

The crystal structures of CF-, CT- and CM-type AB_2O_4 post-spinel phases are composed with one-dimensional double chains of BO_6 octahedra and A cation arrays in tunnel spaces surrounded by the octahedral chains. The CM-type structure is essentially the same as the CT-type except for distortion of the BO_6 octahedra. CF-type AB_2O_4 phases crystallize in wide ranges of ionic radii of A^{2+} and B^{3+}, while CT-type phases crystallize in much narrower cation radius ranges. This fact is consistent with the difference of the tunnel structures, i.e., the A^{2+} site of CF-type is geometrically more flexible than that of CT-type. The relationship between the structure-type and A^{2+} and B^{3+} radii can be used to predict which phase is stable at high pressure. Similarly to the CF-, CT- and CM-types, NAL-type $2/3AB_2O_4{\cdot}1/3CB_2O_4$ phases have the structure consisting of one-dimensional chains of BO_6 octahedra with two kinds of tunnel spaces in which A and C cations are accommodated, respectively, in 6- and 9-fold sites.

In geochemical point of view, stability and phase relations of CF-, CT- and NAL-type phases in simple aluminate-silicate systems and in natural crustal compositions have been precisely determined up to ~ 25 GPa by the large-volume multi-anvil experiments. It has been clarified that the CF-phase accommodates Na^+ in the structures, while the NAL-phase incorporates both of Na^+ and K^+. Because investigations on the precise phase relations above ~25 GPa are quite limited, detailed studies are necessary at pressure up to at least ~50 GPa to clarify the roles of Na^+ and K^+ in the Earth's deep mantle. In addition, investigations on transport properties of CF-, CT- and NAL-type phases in the geochemical systems will be important for understanding of the structure and dynamics of the Earth's interior, because of their potential of high ionic conduction, compared with the other mantle-constituent minerals.

A variety of CF-, CT- and CM-type transition metal oxides have been synthesized at high pressure and high temperature to search for possible ionic conductors and compounds with strongly correlated properties. As described in section "Post-spinel phases in materials science", CF-type $LiMn_2O_4$ and $NaMn_2O_4$ have been synthesized at 4–6 GPa as high ionic conduction materials for candidates of battery cathode materials. The DFT calculation showed that CF-type AMn_2O_4 (A = Li, Na, Mg) compounds have lowest energy barriers than the CT- and CM-type counterparts. Post-spinel-type $NaRu_2O_4$ and $NaRh_2O_4$ synthesized at ~6 GPa exhibit metallic conductivity, and furthermore the latter shows high thermoelectric properties. CF-type NaV_2O_4 synthesized at ~ 6 GPa showed a half-metallic ground state and was proposed as a magnetic topological material.

All the synthesis studies in the view point of materials science have been made at pressures below ~6 GPa. Using the advanced multi-anvil high-pressure technology, synthesis of large-mass materials at pressure up to ~25 GPa is currently much easily made than before. Large single-crystals sufficient for structure analysis and physical property measurements can be synthesized in the whole pressure range described above using the large-volume multi-anvil techniques. The search for novel materials is promising even up to ~50 GPa.

The chemical and physical properties of CT-type phases have yet to be experimentally explored; these phases, which have a different octahedral configuration from the CF-type, are anticipated to exhibit strongly correlated electronic properties, thereby opening up the possibility of uncovering new quantum materials. Also, synthesis studies of novel NAL-type $2/3AB_2O_4{\cdot}1/3CB_2O_4$ phases have not yet been made at high pressures, suggesting that future studies along this direction are desirable.

Novel-structured post-spinel phases, such as those in $MgFe_2O_4$ and $MgAl_2O_4$ described in section "Post-spinel phases in geochemical and mineralogical interest", can be explored by applying the advanced multi-anvil technology, suggesting that further new-structured post-spinel phases and consequently novel chemical and physical properties can be discovered. Future high-pressure research will continue to explore the synthesis of novel post-spinel phases and their potential applications.

Received: 29 April 2024; Accepted: 20 August 2024;
Published online: 27 August 2024

References

1. Ringwood, A. E. *Composition and Petrology of the Earth's Mantle* (McGraw-Hill, 1975).
2. Decker, B. F. & Kasper, J. S. The structure of calcium ferrite. *Acta Cryst.* **10**, 332–337 (1957).
3. Giesber, H. G., Pennington, W. T. & Kolis, J. W. Redetermination of $CaMn_2O_4$. *Acta Cryst. C* **57**, 329–330 (2001).
4. Bertaut, E. F. & Blum, P. Détermination de la structure de Ti_2CaO_4 par la méthode self-consistante d'Approche directe. *Acta Cryst.* **9**, 121–126 (1956).

5. Rogge, M. P. et al. A new synthetic route to pseudo-brookite-type $CaTi_2O_4$. *J. Solid State Chem.* **141**, 338–342 (1998).
6. Yamanaka, T., Uchida, A. & Nakamoto, Y. Structural transition of post-spinel phases $CaMn_2O_4$, $CaFe_2O_4$, and $CaTi_2O_4$ under high pressures up to 80 GPa. *Am. Mineral*. **93**, 1874–1881 (2008). **The article gives detailed description on the crystal structures of the three types of post-spinel phases and exhibits the structural changes with pressure by in situ synchrotron X-ray diffraction method.**
7. Ito, E. & Takahashi, E. Postspinel transformations in the system Mg_2SiO_4-Fe_2SiO_4 and some geophysical implications. *J. Geophys. Res.* **94**, 10637–10646 (1989).
8. Green, D. H., Hibberson, W. O. & Jaques, A. L. Petrogenesis of mid-ocean ridge basalts. in *The Earth, Its Origin, Structure and Evolution* (ed. McElhinney, M. W.) 265–299 (Academic Press, 1979).
9. Taylor, S. R. & McLennan, S. M. *The Continental Crust: Its Composition and Evolution* (Blackwell, 1985).
10. McDonough, W. F. & Sun, S. S. The composition of the earth. *Chem. Geol.* **120**, 223–253 (1995).
11. Irifune, T. & Ringwood, A. E. Phase transformations in subducted oceanic crust and buoyancy relationships at depths of 600-800 km in the mantle. *Earth Planet. Sci. Lett.* **117**, 101–110 (1993).
12. Irifune, T., Ringwood, A. E. & Hibberson, W. O. Subduction of continental crust and terrigenous and pelagic sediments: an experimental study. *Earth Planet. Sci. Lett.* **126**, 351–368 (1994).
13. Hirose, K. & Fei, Y. Subsolidus and melting phase relations of basaltic composition in the uppermost lower mantle. *Geochim. Cosmochim. Acta* **66**, 2099–2108 (2002).
14. Hirose, K., Takafuji, N., Sata, N. & Ohishi, Y. Phase transition and density of subducted MORB crust in the lower mantle. *Earth Planet. Sci. Lett.* **237**, 239–251 (2005).
15. Ohta, K., Hirose, K., Lay, T., Sata, N. & Ohishi, Y. Phase transitions in pyrolite and MORB at lowermost mantle conditions: Implications for a MORB-rich pile above the core–mantle boundary. *Earth Planet. Sci. Lett.* **267**, 107–117 (2008).
16. Ricolleau, A. et al. Phase relations and equation of state of a natural MORB: Implications for the density profile of subducted oceanic crust in the Earth's lower mantle. *J. Geophys. Res.* **115**, B08202 (2010).
17. Ishii, T., Kojitani, H. & Akaogi, M. High-pressure phase transitions and subduction behavior of continental crust at pressure-temperature conditions up to the upper part of the lower mantle. *Earth Planet. Sci. Lett.* **357-358**, 31–41 (2012).
18. Ishii, T., Kojitani, H. & Akaogi, M. Phase relations of harzburgite and MORB up to the uppermost lower mantle conditions: Precise comparison with pyrolite by multi-sample cell high-pressure experiments with implication to dynamics of subducted slabs. *J. Geophys. Res.* **124**, 3491–3507 (2019).
19. Ishii, T. et al. High pressure-temperature phase relations of basaltic crust up to mid-mantle conditions. *Earth Planet. Sci. Lett.* **584**, 117472 (2022).
20. Guinot, N. & Andrault, D. Equations of state of Na-K-Al host phases and implications for MORB density in the lower mantle. *Phys. Earth Planet. Inter.* **143-144**, 107–128 (2004).
21. Miura, H. et al. Crystal structure of $CaMg_2Al_6O_{12}$, a new Al-rich high pressure form. *Am. Mineral*. **85**, 1799–1803 (2000). **The article gives the first structure analysis and characterization of the hexagonal aluminous NAL phase with implications to the Earth's mantle.**
22. Mao, H. K. & Mao, W. L. Theory and practice: diamond-anvil cells and probes for high-P–T mineral physics studies. in *Treatise on Geophysics* (eds. Price, G. D. & Stixrude, L.) 263–291 (Elsevier, 2007).
23. Ito, E. Multi-anvil cells and high pressure experimental methods in Mineral Physics. in *Treatise on* Geophysics (eds. Price, G. D. & Stixrude, L.) 233–261 (Elsevier, 2015). **The article provides a comprehensive review on experimental methods of multi-anvil apparatus with applications to material synthesis and physical property measurements at high pressure and high temperature, including applications to geoscience.**
24. Akaogi, M. High-pressure and high-temperature experiments with large-volume apparatus. in *High-Pressure Silicates and Oxides—Phase Transition and Thermodynamics* (M. Akaogi) 25–46 (Springer, 2022).
25. Akaogi, M., Yusa, H., Shiraishi, K. & Suzuki, T. Thermodynamic properties of α-quartz, coesite, and stishovite and equilibrium phase relations at high pressures and high temperatures. *J. Geophys. Res.* **100**, 22337–22347 (1995).
26. Akaogi, M., Takayama, H., Kojitani, H., Kawaji, H. & Atake, T. Low-temperature heat capacities, entropies and enthalpies of Mg_2SiO_4 polymorphs, and α-β-γ and postspinel phase relations at high pressure. *Phys. Chem. Miner.* **34**, 169–183 (2007).
27. Akaogi, M., Kojitani, H., Morita, T., Kawaji, H. & Atake, T. Low-temperature heat capacities, entropies and high-pressure phase relations of $MgSiO_3$ ilmenite and perovskite. *Phys. Chem. Miner.* **35**, 287–297 (2008).
28. Akaogi, M., Oohata, M., Kojitani, H. & Kawaji, H. Thermodynamic properties of stishovite by low-temperature heat capacity measurements and the coesite-stishovite transition boundary. *Am. Mineral.* **96**, 1325–1330 (2011).
29. Atake, T., Inoue, N., Kawaji, H., Matsuzaka, K. & Akaogi, M. Low temperature heat capacity of high-pressure phase of SiO_2, coesite, and calculation of the α-quartz-coesite equilibrium boundary. *J. Chem. Thermodyn.* **32**, 217–227 (2000).
30. Kojitani, H., Ishii, T. & Akaogi, M. Thermodynamic investigation on phase equilibrium boundary between calcium ferrite-type $MgAl_2O_4$ and $MgO + α\text{-}Al_2O_3$. *Phys. Earth Planet. Inter.* **212–213**, 100–105 (2012).
31. Kojitani, H., Inoue, T. & Akaogi, M. Precise measurements of enthalpy of post-spinel transition in Mg_2SiO_4 and application to the phase boundary calculation. *J. Geophys. Res.* **121**, 729–742 (2016).
32. Irifune, T., Kurio, A., Sakamoto, S., Inoue, T. & Sumiya, H. Ultrahard polycrystalline diamond from graphite. *Nature* **421**, 599–600 (2003).
33. Irifune, T., Isobe, F. & Shimei, T. A novel large-volume Kawai-type apparatus and its application to the synthesis of sintered bodies of nano-polycrystalline diamond. *Phys. Earth Planet. Inter.* **228**, 255–261 (2014).
34. Kawazoe, T., Buchen, J. & Marquardt, H. Synthesis of large wadsleyite single crystals by solid-state recrystallization. *Am. Mineral.* **100**, 2336–2339 (2015).
35. Ishii, T., Criniti, G., Wang, X., Glazyrin, K. & Ballaran, T. B. Synthesis and structural analysis of $CaFe_2O_4$-type single crystals in the $NaAlSiO_4$-$MgAl_2O_4$-Fe_3O_4 system. *Am. Mineral.* **108**, 217–221 (2023).
36. Satta, N. et al. High-pressure elasticity of δ-(Al,Fe)OOH single crystals and seismic detectability of hydrous MORB in the shallow lower mantle. *Geophys. Res. Lett.* **48**, e2021GL094185 (2021).
37. Su, X. et al. Spectroscopic evidence for the Fe^{3+} spin transition in iron-bearing δ-AlOOH at high pressure. *Am. Mineral.* **106**, 1709–1716 (2021).
38. Rubie, D. C., Karato, S., Yan, H. & O'Neill, H. S. C. Low differential stress and controlled chemical environment in multianvil high-pressure experiments. *Phys. Chem. Miner.* **20**, 315–322 (1993).
39. Yamada, I. et al. A perovskite containing quadrivalent iron as a charge-disproportionated ferrimagnet. *Angew. Chem.* **120**, 7140–7143 (2008).
40. Ishii, T., McCammon, C. & Katsura, T. Iron and aluminum substitution mechanism in the perovskite phase in the system $MgSiO_3$-$FeAlO_3$-MgO. *Am. Mineral.* **108**, 738–743 (2023).

41. Shatskiy, A. et al. Growth of large (1 mm) $MgSiO_3$ perovskite single crystals: A thermal gradient method at ultrahigh pressure. *Am. Mineral.* **92**, 1744–1749 (2007).
42. Kawazoe, T. et al. Single crystal synthesis of δ-(Al,Fe)OOH. *Am. Mineral.* **102**, 1953–1956 (2017).
43. Yamaura, K. et al. NaV_2O_4: a quasi-1D metallic antiferromagnet with half-metallic chains. *Phys. Rev. Lett.* **99**, 196601 (2007). **The article reports that a flux-grown single crystal in NaV_2O_4 under high pressure has the $CaFe_2O_4$-type structure with remarkable correlated electron properties.**
44. Wang, Y. et al. The large-volume high-pressure facility at GSECARS: a "Swiss-army-knife" approach to synchrotron-based experimental studies. *Phys. Earth Planet. Inter.* **174**, 270–281 (2009).
45. Liu, Z. et al. Stability and solubility of the $FeAlO_3$ component in bridgmanite at uppermost lower mantle conditions. *J. Geophys. Res.* **125**, e2019JB018447 (2020).
46. Ishii, T. et al. Pressure generation to 65 GPa in a Kawai-type multi-anvil apparatus with tungsten carbide anvils. *High Press Res.* **37**, 507–515 (2017).
47. Ishii, T., Liu, Z. & Katsura, T. A breakthrough in pressure generation by a Kawai-type multi-anvil apparatus with tungsten carbide anvils. *Engineering* **5**, 434–440 (2019). **The article reviews the most advanced multi-anvil technology that allows to make access easier to material synthesis at ultra-high pressure over 40 GPa and introduces their applications to geoscience.**
48. Ishii, T. et al. Synthesis and crystal structure of $LiNbO_3$-type $Mg_3Al_2Si_3O_{12}$: a possible indicator of shock conditions of meteorites. *Am. Mineral.* **102**, 1947–1952 (2017).
49. Ishii, T. et al. High-pressure syntheses and crystal structure analyses of a new low-density $CaFe_2O_4$-related and $CaTi_2O_4$-type $MgAl_2O_4$ phases. *Am. Mineral.* **106**, 1105–1112 (2021).
50. Kojitani, H., Hisatomi, R. & Akaogi, M. High-pressure phase relations and crystal chemistry of calcium ferrite-type solid solutions in the system $MgAl_2O_4$-Mg_2SiO_4. *Am. Mineral.* **92**, 1112–1118 (2007).
51. Ishii, T. et al. High-pressure phase relations and crystal structures of new post-spinel phases in MgV_2O_4, FeV_2O_4, and $MnCr_2O_4$: Crystal chemistry of AB_2O_4 post-spinel compounds. *Inorg. Chem.* **57**, 6648–6657 (2018).
52. Haavik, C., Stølen, S., Fjellvag, H., Hanfland, M. & Hausermann, D. Equation of state of magnetite and its high-pressure modification: thermodynamics of the Fe-O system at high pressure. *Am. Mineral.* **85**, 514–523 (2000).
53. Enomoto, A., Kojitani, H., Akaogi, M., Miura, H. & Yusa, H. High-pressure transitions in $MgAl_2O_4$ and a new high-pressure phase of $Mg_2Al_2O_5$. *J. Solid State Chem.* **182**, 389–395 (2009).
54. Ishii, T. et al. High-pressure phase transitions in $FeCr_2O_4$ and structure analysis of new post-spinel $FeCr_2O_4$ and $Fe_2Cr_2O_5$ phases with meteoritical and petrological implications. *Am. Mineral.* **99**, 1788–1797 (2014).
55. Woodland, A. B., Frost, D. J., Trots, D. M., Klimm, K. & Mezouar, M. In situ observation of the breakdown of magnetite (Fe_3O_4) to Fe_4O_5 and hematite at high pressures and temperatures. *Am. Mineral.* **97**, 1808–1811 (2012).
56. Irifune, T., Fujino, K. & Ohtani, E. A new high-pressure form of $MgAl_2O_4$. *Nature* **349**, 409–411 (1991).
57. Akaogi, M., Hamada, Y., Suzuki, T., Kobayashi, M. & Okada, M. High pressure transitions in the system $MgAl_2O_4$-$CaAl_2O_4$: a new hexagonal aluminous phase with implication for the lower mantle. *Phys. Earth Planet. Inter.* **115**, 67–77 (1999).
58. Kojitani, H. et al. High pressure high temperature phase relations in $MgAl_2O_4$. *J. Phys. Conf. Ser.* **215**, 012098 (2010).
59. Funamori, N. et al. High-pressure transformations in $MgAl_2O_4$. *J. Geophys. Res.* **103**, 20813–20818 (1998).
60. Ono, S., Kikegawa, T. & Ohishi, Y. The stability and compressibility of $MgAl_2O_4$ high-pressure polymorphs. *Phys. Chem. Miner.* **33**, 200–206 (2006).
61. Man, L. et al. Alumina solubility in periclase determined to lower mantle conditions and implications for ferropericlase inclusions in diamonds. *Geochim. Cosmochim. Acta* **375**, 36–49 (2024).
62. Akaogi, M., Tanaka, A., Kobayashi, M., Fukushima, N. & Suzuki, T. High-pressure transformations in $NaAlSiO_4$ and thermodynamic properties of jadeite, nepheline, and calcium ferrite-type phase. *Phys. Earth Planet. Inter.* **130**, 49–58 (2002).
63. Ishii, T. et al. Discovery of new-structured post-spinel $MgFe_2O_4$: Crystal structure and high-pressure phase relations. *Geophys. Res. Lett.* **47**, e2020GL087490 (2020).
64. Kimura, F., Kojitani, H. & Akaogi, M. High-pressure and high-temperature phase relations in the systems $KAlSiO_4$-$MgAl_2O_4$ and $CaAl_2O_4$-$MgAl_2O_4$: stability fields of NAL phases. *Phys. Earth Planet. Inter.* **310**, 106632 (2021).
65. Ono, A., Akaogi, M., Kojitani, H., Yamashita, K. & Kobayashi, M. High-pressure phase relations and thermodynamic properties of hexagonal aluminous phase and calcium-ferrite phase in the systems $NaAlSiO_4$-$MgAl_2O_4$ and $CaAl_2O_4$-$MgAl_2O_4$. *Phys. Earth Planet. Inter.* **174**, 39–49 (2009).
66. Kojitani, H., Iwabuchi, T., Kobayashi, M., Miura, H. & Akaogi, M. Structure refinement of high-pressure hexagonal aluminous phases $K_{1.00}Mg_{2.00}Al_{4.80}Si_{1.15}O_{12}$ and $Na_{1.04}Mg_{1.88}Al_{4.64}Si_{1.32}O_{12}$. *Am. Mineral.* **96**, 1248–1253 (2011).
67. Miyajima, N. et al. Potential host phase of aluminum and potassium in the Earth's lower mantle. *Am. Mineral.* **86**, 740–746 (2001).
68. Perrillat, J. P. et al. Phase transformations of subducted basaltic crust in the upmost lower mantle. *Phys. Earth Planet. Inter.* **157**, 139–149 (2006).
69. Kuwahara, H. & Nakada, R. Partitioning of Fe^{2+} and Fe^{3+} between bridgmanite and silicate melt: implications for redox evolution of the Earth's mantle. *Earth Planet. Sci. Lett.* **615**, 118197 (2023).
70. Sun, W. et al. K- and Na-rich davemaoite inclusion in diamond is not inherited from deeply subducted oceanic crusts. *Earth Planet. Sci. Lett.* **637**, 118741 (2024).
71. Stacey, F. D. & Davis, P. M. *Physics of the Earth* (Cambridge Univ. Press, 2008).
72. Kato, C., Hirose, K., Komabayashi, T., Ozawa, H. & Ohishi, Y. NAL phase in K-rich portions of the lower mantle. *Geophys. Res. Lett.* **40**, 5085–5088 (2013).
73. Murthy, V. R., van Westrenen, W. & Fei, Y. Experimental evidence that potassium is a substantial radioactive heat source in planetary cores. *Nature* **423**, 163–165 (2003).
74. Yoshino, T. & Katsura, T. Electrical conductivity of mantle minerals: Role of water in conductivity anomalies. *Annu. Rev. Earth Planet. Sci.* **41**, 605–628 (2013).
75. Shannon, R. D. Revised effective ionic radii and systematic studies of interatomic distances in halides and chaleogenides. *Acta Cryst.* **A32**, 751–767 (1976).
76. Catti, M. High-pressure stability, structure and compressibility of *Cmcm* $MgAl_2O_4$: an ab initio study. *Phys. Chem. Miner.* **28**, 729–736 (2001).
77. Caracas, R. & Banigan, E. J. Elasticity and Raman and infrared spectra of $MgAl_2O_4$ spinel from density functional perturbation theory. *Phys. Earth Planet. Inter.* **174**, 113 (2009).
78. López, S., Romero, A. H., Rodríguez-Hernández, P. & Muñoz, A. First-principles study of the high-pressure phase transition in $ZnAl_2O_4$ and $ZnGa_2O_4$: From cubic spinel to orthorhombic post-spinel structures. *Phys. Rev. B* **79**, 214103 (2009).
79. Errandonea, D., Kumar, R. S., Manjón, F. J., Ursaki, V. V. & Rusu, E. V. Post-spinel transformations and equation of state in $ZnGa_2O_4$: Determination at high pressure by in situ x-ray diffraction. *Phys. Rev. B* **79**, 024103 (2009).

80. Byles, B. W., Palapati, N. K. R., Subramanian, A. & Pomerantseva, E. The role of electronic and ionic conductivities in the rate performance of tunnel structured manganese oxides in Li-ion batteries. *APL Mater.* **4**, 046108 (2016).
81. Matsuda, Y. et al. Synthesis, crystal structure, and ionic conductivity of tunnel structure phosphates, $RbMg_{1-x}H_{2x}(PO_3)_3{\cdot}y(H_2O)$. *J. Mater. Chem. A* **1**, 15544–15551 (2013).
82. Yamaura, K. et al. Spinel-to-$CaFe_2O_4$-type structural transformation in $LiMn_2O_4$ under high pressure. *J. Am. Chem. Soc*. **128**, 9448–9456 (2006). **The article reports high-pressure synthesis of a new dense form of $LiMn_2O_4$ with the $CaFe_2O_4$-type structure, offering insights into ionic conduction and the post-spinel phases of geomaterials.**
83. Mukai, K., Uyama, T. & Yamada, I. Structural and electrochemical analyses on the transformation of $CaFe_2O_4$-type $LiMn_2O_4$ from spinel-type $LiMn_2O_4$. *ACS Omega* **4**, 6459–6467 (2019).
84. Akimoto, J. & Takei, H. Synthesis and crystal structure of $NaTi_2O_4$: A new mixed-valence sodium titanate. *J. Solid State Chem.* **79**, 212–217 (1989).
85. Liu, X. et al. High stable post-spinel $NaMn_2O_4$ cathode of sodium ion battery. *J. Mater. Chem. A* **2**, 14822–14826 (2014).
86. Malavasi, L., Tealdi, C., Flor, G. & Amboage, M. High-pressure stability of tetragonal spinel $MgMn_2O_4$: Role of inversion. *Phys. Rev. B* **71**, 174102 (2005).
87. Ling, C. & Mizuno, F. Phase stability of post-spinel compound AMn_2O_4 (A = Li, Na, or Mg) and its application as a rechargeable battery cathode. *Chem. Mater.* **25**, 3062–3071 (2013).
88. Hancock, J. C. et al. Expanding the ambient-pressure phase space of $CaFe_2O_4$-type sodium postspinel host-guest compounds. *ACS Org. Inorg. Au* **2**, 8–22 (2022).
89. Hancock, J. C. et al. Electrochemistry in the large tunnels of lithium postspinel compounds. *Chem. Mater.* **36**, 4616–4630 (2024).
90. Foo, M. L. et al. Synthesis and characterization of the pseudo-hexagonal hollandites $ALi_2Ru_6O_{12}$ (*A* = Na, K). *J. Solid State Chem.* **179**, 941–948 (2006).
91. Yamada, H., Matsui, Y. & Ito, E. Crystal-chemical characterization of $NaAlSiO_4$ with the $CaFe_2O_4$ structure. *Mineral. Mag.* **47**, 177–181 (1983).
92. Akimoto, J. et al. High-pressure synthesis and crystal structure analysis of $NaMn_2O_4$ with the calcium ferrite-type structure. *J. Solid State Chem.* **179**, 169–174 (2006).
93. Mizoguchi, H., Zakharov, L. N., Marshall, W. J., Sleight, A. W. & Subramanian, M. A. $AA'_2Rh_6O_{12}$: a new family of rhodium oxides exhibiting high thermopower coupled with high electrical conductivity. *Chem. Mater.* **21**, 994–999 (2009).
94. Yogi, A. K. et al. Coexisting Z-type charge and bond order in metallic $NaRu_2O_4$. *Commun. Mater.* **3**, 3 (2022). **The discovery of coexisting dimerization and charge ordering within dimers in metallic $NaRu_2O_4$ highlights the intricate interplay among orbital, charge, and lattice degrees of freedom in the post-spinel-type materials.**
95. Regan, K. A., Huang, Q., Lee, M., Ramirez, A. P. & Cava, R. J. Structure and magnetism of $NaRu_2O_4$ and $Na_{2.7}Ru_4O_9$. *J. Solid State Chem.* **179**, 195–204 (2006).
96. Yamaura, K. et al. High-pressure synthesis, crystal structure determination, and a Ca substitution study of the metallic rhodium oxide $NaRh_2O_4$. *Chem. Mater.* **17**, 359–365 (2005).
97. Rahnamaye Aliabad, H. A. & Hosseini, N. Effect of substituted Ca on the thermoelectric and optoelectronic properties of $NaRh_2O_4$ under pressure. *J. Electr. Mater.* **47**, 2009–2016 (2018).
98. He, T. et al. Structure, phase stability, half-metallicity, and fully spin-polarized Weyl states in compound NaV_2O_4: An example for topological spintronic material. *Phys. Rev. Mater.* **5**, 024205 (2021).
99. Ishii, T. et al. High-pressure high-temperature transitions in $MgCr_2O_4$ and crystal structures of new $Mg_2Cr_2O_5$ and post-spinel $MgCr_2O_4$ phases with implications for ultra-high pressure chromitites in ophiolites. *Am. Mineral.* **100**, 59–65 (2015).
100. Lazic, B., Kahlenberg, V., Konzett, J. & Kaindl, R. On the polymorphism of $CaAl_2O_4$ - structural investigations of two high pressure modifications. *Solid State Sci.* **8**, 589–597 (2006).
101. Ross, C. R. II, Rubie, D. C. & Paris, E. Rietveld refinement of the high-pressure polymorph of Mn_3O_4. *Am. Mineral.* **75**, 1249–1252 (1990).
102. Darul, J., Lathe, C. & Piszora, P. Mn_3O_4 under high pressure and temperature: thermal stability, polymorphism, and elastic properties. *J. Phys. Chem.* **117**, 23487–23494 (2013).
103. Niazi, A. et al. Single-crystal growth, crystallography, magnetic susceptibility, heat capacity, and thermal expansion of the antiferromagnetic *S* = 1 chain compound CaV_2O_4. *Phys. Rev. B* **79**, 104432 (2009).
104. Hadermann, J., Abakumov, A. M., Gillie, L. J., Martin, C. & Hervieu, M. Coupled cation and charge ordering in the $CaMn_3O_6$ tunnel structure. *Chem. Mater.* **18**, 5530–5536 (2006).
105. Michel, C. et al. $SrTl_2O_4$, a semi-metal with the $CaFe_2O_4$ structure. *Mater. Res. Bull.* **26**, 123–128 (1991).
106. Karunadasa, H. et al. Honeycombs of triangles and magnetic frustration in SrL_2O_4 (L= Gd, Dy, Ho, Er, Tm, and Yb). *Phys. Rev. B Condens. Matter Mater. Phys.* **71**, 144414 (2005).
107. Besara, T. et al. Single crystal synthesis and magnetism of the $BaLn_2O_4$ family (*Ln* = lanthanide). *Prog. Solid State Chem.* **42**, 23–36 (2014).
108. Bruno, S. R., Blakely, C. K. & Poltavets, V. V. Novel $LiFeTiO_4$ polymorph with a tunnel structure: synthesis, structural and electrochemical characterization. *ECS Trans.* **41**, 29–34 (2012).
109. Viciu, L., Ryser, A., Mensing, C. & Bos, J. W. G. Ambient-pressure synthesis of two new vanadium-based calcium ferrite-type compounds: $NaV_{1.25}Ti_{0.75}O_4$ and $NaVSnO_4$. *Inorg. Chem.* **54**, 7264–7271 (2015).
110. Ishiguro, T. et al. Non-stoichiometric sodium iron(II) titanium(IV) oxide. *Acta Cryst. B* **34**, 3346–3348 (1978).
111. Mizoguchi, H. et al. New $A_{2/3-x}Rh_2O_4$ compounds with the $CaFe_2O_4$ structure where A is a rare earth or Bi. *Inorg. Chem.* **48**, 204–208 (2009).
112. Reid, A. F., Wadsley, A. D. & Ringwood, A. E. High pressure $NaAlGeO_4$, a calcium ferrite isotype and model structure of silicates at depth in the earth's mantle. *Acta Cryst.* **23**, 736–739 (1967).
113. Greenberg, E. et al. High-pressure magnetic, electronic, and structural properties of MFe_2O_4 (*M* = Mg, Zn, Fe) ferric spinels. *Phys. Rev. B* **95**, 195150 (2017).
114. Ohgushi, K., Gotou, H., Yagi, T. & Ueda, Y. High-pressure synthesis and magnetic properties of orthorhombic $CuRh_2O_4$. *J. Phys. Soc. Jpn.* **75**, 023707 (2006).
115. Wang, X. et al. High-pressure synthesis, crystal structure, and electromagnetic properties of $CdRh_2O_4$: an analogous oxide of the postspinel mineral $MgAl_2O_4$. *Inorg. Chem.* **51**, 6868–6875 (2012).
116. Arévalo-López, A. M., Dos santos-García, A. J., Castillo-Martínez, E., Durán, A. & Alario-Franco, M. A. Spinel to $CaFe_2O_4$ transformation: mechanism and properties of β-$CdCr_2O_4$. *Inorg. Chem.* **49**, 2827–2833 (2010).
117. Shizuya, M., Isobe, M. & Takayama-Muromachi, E. Structure and properties of the $CaFe_2O_4$-type cobalt oxide $CaCo_2O_4$. *J. Solid State Chem.* **180**, 2550–2557 (2007).
118. Momma, K. & Izumi, F. VESTA 3 for three-dimensional visualization of crystal, volumetric and morphology data. *J. Appl. Cryst.* **44**, 1272–1276 (2011).
119. Müller-Buschbaum, H. K. Über Oxoscandate. II. Zur Kenntnis des $MgSc_2O_4$. *Zeit Anorg. Allg. Chem.* **343**, 113–120 (1966).

120. Hoerkner, W. & Müller-Buschbaum, H. K. Einkristalluntersuchungen von β-$CaCr_2O_4$. *Zeit Naturforsch. B* **31**, 1710–1711 (1976).
121. Müller-Buschbaum, H. K. & Schnering, H. G. ÜberOxoscandate I. Zur Kenntnis des $CaSc_2O_4$. *Zeit Anorg. Allg. Chem.* **336**, 295–305 (1965).
122. Müller-Buschbaum, H. K. & Von Schenck, R. Untersuchungen an $SrYb_2O_4$, $CaYb_2O_4$ und $CaLu_2O_4$; ein Beitrag zur Kristallstruktur des Calciumferrat(III)-Typs. *Zeit Anorg. Allg. Chem.* **377**, 70–78 (1970).
123. Wang, S., Ma, S., Wu, J., Ye, Z. & Cheng, X. A promising temperature sensing strategy based on highly sensitive Pr^{3+}-doped $SrRE_2O_4$ (RE = Sc, Lu and Y) luminescent thermometers. *Chem. Eng. J.* **393**, 124564 (2020).

Acknowledgements

The authors thank Hiroshi Kojitani for his help to conduct the studies on post-spinel phases. This research was supported in part by the Grants-in-Aid of the Scientific Research of the Japan Society for the Promotion of Science (JSPS), nos. 25287145 and 17H02986 to M.A., JP23K19067 to T.I., and JP22H04601 and JP20H05276 to K.Y., and by the MEXT-supported program for the Strategic Research Foundation at Private Universities. MANA is supported by World Premier International Research Center Initiative (WPI), MEXT, Japan.

Author contributions

M.A. conceived the manuscript. M.A., T.I., and K.Y. equally contributed in writing the manuscript.

Competing interests

The authors declare no competing interests.

Additional information

Supplementary information The online version contains supplementary material available at https://doi.org/10.1038/s42004-024-01278-0.

Correspondence and requests for materials should be addressed to Masaki Akaogi.

Peer review information *Communications Chemistry* thanks Kent J Griffith and the other, anonymous, reviewer(s) for their contribution to the peer review of this work. A peer review file is available.